T_1 Thermometry for Deep Brain Stimulation Applications: A Comparison between Rapid Gradient Echo Sequences

Zinat Zarrini-Monfared (PhD Candidate)[1], Mansour Parvaresh (MD)[2], Mehdi Mohammad Mirbagheri (PhD)[1,3]*

[1]Department of Medical Physics and Biomedical Engineering, School of Medicine, Tehran University of Medical Sciences, Tehran, Iran
[2]Department of Neurosurgery, Hazrat Rasool Hospital, Iran University of Medical Sciences, Tehran, Iran
[3]Department of Physical Medicine and Rehabilitation, Northwestern University, USA

ABSTRACT

Background: T_1 thermometry is considered a straight method for the safety monitoring of patients with deep brain stimulation (DBS) electrodes against radiofrequency-induced heating during Magnetic Resonance Imaging (MRI), requiring different sequences and methods.

Objective: This study aimed to compare two T_1 thermometry methods and two low specific absorption rate (SAR) imaging sequences in terms of the output image quality.

Material and Methods: In this experimental study, a gel phantom was prepared, resembling the brain tissue properties with a copper wire inside. Two types of rapid gradient echo sequences, namely radiofrequency-spoiled and balanced steady-state free precession (bSSFP) sequences, were used. T_1 thermometry was performed by either T_1-weighted images with a high SAR sequence to increase heating around the wire or T_1 mapping methods.

Results: The balanced steady-state free precession (bSSFP) sequence provided higher image quality in terms of spatial resolution ($1\times1\times1.5$ mm^3 compared with $1\times1\times3$ mm^3) at a shorter acquisition time. The susceptibility artifact was also less pronounced for the bSSFP sequence compared with the radiofrequency-spoiled sequence. A temperature increase, of up to 8 °C, was estimated using a high SAR sequence. The estimated change in temperature was reduced when using the T_1 mapping method.

Conclusion: Heating induced during MRI of implanted electrodes could be estimated using high-resolution T_1 maps obtained from inversion recovery bSSFP sequence. Such a method gives a direct estimation of heating during the imaging sequence, which is highly desirable for safe MRI of DBS patients.

Citation: Zarrini-Monfared Z, Parvaresh M, Mirbagheri MM. T_1 Thermometry for Deep Brain Stimulation Applications: A Comparison between Rapid Gradient Echo Sequences. *J Biomed Phys Eng*. 2024;14(6):569-578. doi: 10.31661/jbpe.v0i0.2210-1546.

Keywords

Magnetic Resonance Imaging; Safety; Thermometry; Deep Brain Stimulation

Introduction

Deep brain stimulation (DBS) involves inserting long leads into the brain to stimulate specific targets in a variety of diseases, including Parkinson's disease, essential tremor, and drug resistance epilepsy [1]. The targets, such as the subthalamic nucleus (STN) and globus pallidus interna (GPi) are miniscule and hardly seen by common imaging techniques. In this way, Magnetic Resonance Imaging (MRI) provides various advantages in the localization of the target for

*Corresponding author:
Mehdi Mohammad Mirbagheri
Department of Physical Medicine and Rehabilitation, Northwestern University, USA
E-mail:
mehdi.northwestern@gmail.com

Received: 2 October 2022
Accepted: 15 December 2022

surgery guidance, monitoring the progress of treatment after surgery, and DBS training [2]. Functional MRI (fMRI) can provide a unique opportunity in finding new functional targets, evaluating outcomes, and shedding light on the underlying mechanisms of DBS therapy [1]. These benefits can be achieved only if patient safety is fully considered in the MRI environment [3].

There are different MRI-related safety issues, among which heat generation near the electrode is the main concern for DBS implants [3]. DBS implants are usually MRI-compatible under certain conservative conditions [4], restricting the potential benefits of MRI. However, there is considerable evidence, showing that these safety recommendations are unnecessarily conservative [5, 6], and the specific absorption rate (SAR) reported by the scanner may not appropriately represent the amount of heat in this situation [3, 7, 8]. On the other hand, numerous factors affect the heating process, varying the amount of produced heat in different situations [3, 9]. Direct temperature measurement using MRI thermometry [10, 11] is suggested to provide 2D or 3D thermal maps noninvasively in this situation.

Various magnetic resonance (MR) parameters, including T_1, T_2, proton resonance frequency, and diffusion coefficient are temperature sensitive [10]. The proton resonance frequency and T_1 have higher temperature sensitivity and at lower magnetic fields, T_1 thermometry is more sensitive [10], and T_1-weighted images are also used for target localization and treatment evaluation [12]. Consequently, T_1 thermometry seems to be pertinent to temperature measurement in patients with DBS implants [13].

Despite better management of the susceptibility artifact, the spin echo (SE) sequence is not recommended for patients with DBS electrodes because of the high RF power deposition during refocusing [14]. Two gradient-echo sequences have been used for T_1 thermometry [10, 13]: the RF-spoiled and the balanced steady-state free precession (bSSFP) sequences, commercially called FLASH and TrueFISP, respectively [15]. However, FLASH is more common for neuroimaging, TrueFISP can be less sensitive to the susceptibility artifact [16], resulting in a good candidate for DBS patients.

Magnetic resonance thermometry has been performed using different methods [13, 17, 18]. The extra amount of heat is usually generated by modifying the sequence [17], applying a high SAR sequence [18], or repeating the sequence multiple times [13] to increase the imaging sensitivity. Temperature changes could be detected by alterations in signal intensity of T_1-weighted images in comparison with a reference image [13]. The extra amount of heat generated by the above-mentioned methods can be clinically harmful. On the other hand, it overestimates the amount of heat produced by the imaging sequence. In a second approach, temperature distribution could be obtained from alterations in T_1 values of a T_1 map [10]. T_1 mapping is usually performed using a set of images at different inversion times (TI) and a fitting method [19, 20]. Since the amount of heat is almost independent of TI [21], it remains unchanged for all images in a specific set. A precise T_1 map could thus provide temperature distribution around the wire during MRI.

The study aims to compare two gradient-echo sequences (i.e., FLASH and TrueFISP) for T_1 thermometry in a phantom with a metal wire inside. To the best of our knowledge, a comparison between these two approaches has not been previously reported. Consequently, the obtained results can help develop safety protocols in clinical situations.

Material and Methods

Phantom

In this experimental study, all the measurements were performed on a gel phantom [22] with magnetic resonance and electrical prop-

erties similar to those of human tissues. Agarose (*Type I, Merck*) (0.755 g) as a T_2 modifier was mixed with 23.7 µmol / kg $GdCl_3$ (*Sigma-Aldrich*) as a T_1 modifier and 3 gr carrageenan (*Sigma-Aldrich*) as a gelling agent. Distilled and deionized water was added to bring the total mass to 100 g to provide the MR properties equivalent to the thalamus [22]. The mixture was then stirred and simultaneously heated in a boiling bath at a temperature of 90 °C. Finally, the solution was boiled in a microwave oven and poured into 100 ml Pyrex bottles for solidification.

A thin copper wire (1.2 mm in diameter), which was electrically insulated except for 1.5 mm at one end as an electrode with a 1-mm distance from the wire tip (Figure 1), was used as the lead. Before the phantom got solidified, the wire was placed into it. The susceptibility artifact is supposed to be less significant because of the close magnetic susceptibility of the copper to that of water [17]. The length of the wire was 90 cm, at which the most heat generation is expected in a 3 T MRI scanner [23]. Only the last 50 mm of wire was placed into the phantom. The external portion of the wire was put straight into the head coil without looping to increase heat [24, 25]. A thin and straight wire can cause more heating than a configuration of coiled wire resembling real electrodes [26]. Accordingly, a worst-case scenario is presented in this study. The phantoms were then placed in the MRI room 24 h before the experiment to assure thermal equilibrium.

The T_1 and T_2 relaxation times of the phantom were measured using saturation-recovery spin-echo and multi-echo methods, respectively [19]. The dielectric properties of the phantom were measured before solidification using an Agilent 85070E Dielectric probe kit. The probe was calibrated with water, and the measurement was also performed three times (Table 1).

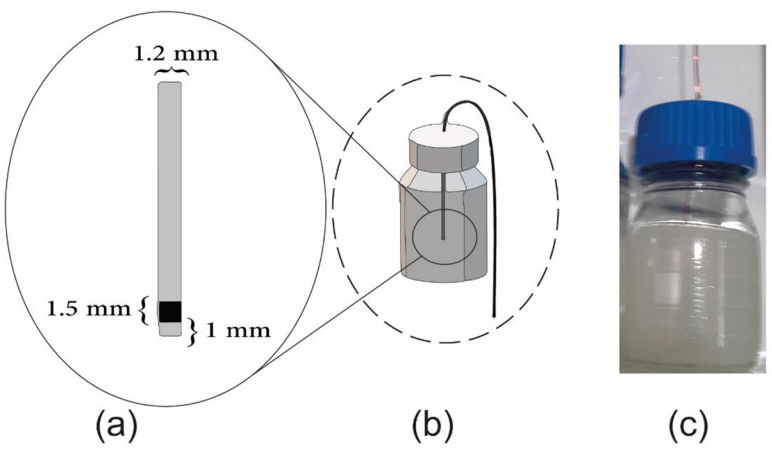

Figure 1: (**a**) Schematic of the copper wire inside the phantom, (**b**) Schematic of the phantom in a Pyrex bottle, and (**c**) The phantom image.

Table 1: Phantom properties at 64 MHz (1.5 T).

T_2 (ms)	T_1 (ms)	[a]σ (S/m)	[b]ε_r	NaCl (%)	Agar (%)	$GdCl_3$ (µ mol/kg)
125	890	0.241	74.7	0	0.755	23.7

[a] conductivity, [b] relative permittivity

MRI imaging

All the measurements were performed on a 3 T *Siemens Prisma* scanner (*Siemens Healthineers, Muenchen, Germany*). Two approaches were used for T_1 thermometry, and two gradient-echo sequences (FLASH and TrueFISP) were utilized for each approach. The image acquisition time was kept at less than 15 min for all the experiments.

First approach

A reference T_1-weighted image was obtained before a high SAR turbo spin echo (TSE) sequence. The high SAR sequence was used to induce heating around the wire. Immediately after the TSE sequence acquisition, a second T_1-weighted image was acquired to compare with the reference image. A difference image was obtained by subtracting the two T_1-weighted images. The parameters of the TSE sequence were modified for a whole head averaged SAR of 2.23 W/kg (reported by the MRI scanner) during a scan time of approximately 1 min.

The T_1-weighted images were acquired using FLASH or TrueFISP sequences, and the imaging parameters were modified to maximize the SNR of the sequence based on the analytical expressions available for signal intensity in the literature [16, 20, 27, 28]. In TrueFISP, the SNR is almost independent of TR for $TR<<T_2$ [28]; TR was thus considered as low as possible. The shortest TE was selected for both sequences to keep the susceptibility artifact as low as possible. The parameters for each sequence are shown in Table 2.

Second approach

T_1 was measured near the wire tip, and the temperature was estimated according to the T_1 changes in that area. The FLASH and TrueFISP were used with an inversion-recovery preparation pulse for T_1 mapping, and the Levenburg-Marquardt method was used for data fitting for the available real images. For magnitude images, a data fitting method [29] was used due to signal polarity concerns. Three TIs with values specified in [30] were used to optimize precision per unit of time.

A T_1 mapping method independent of the real flip angle field [31] for FLASH was here used with the following parameters: *TR/TE*: 1020/2.36 ms, slice thickness: 4 mm, TI: [30, 200, 1000] ms, and a flip angle of 8°. For TrueFISP, a linear phase encoding direction was used to ascertain the steady state condition for the central lines of the k-space. The imaging parameters were as follows: *TR/TE*: 5000/1.96 ms, slice thickness: 3 mm, TI: [320, 820, 1100, 4100] ms, and a flip angle of 34°. For both sequences, the average was set to 4 to have detectable data.

Results

The phantom properties are summarized in Table 1.

First approach

The sequence parameters for the first thermometry approach are presented in Table 2.

The difference images for two adjacent slices containing the wire tip are shown in

Table 2: Imaging parameters for each sequence in the first approach.

Sequence	FLASH	TrueFISP
Width	256	256
Height	256	256
In-plane resolution	1 mm, isotropic	1 mm, isotropic
Slice thickness (mm)	3	1.5
***TR* (ms)**	6.2	4.63
***TE* (ms)**	2.36	2.32
No of averages	4	4
Flip angle (deg)	6	38

FLASH: Fast Low-Angle Shot, TrueFISP: True Fast Imaging with Steady Precession, TR: Repetition Time, TE: Echo Time

Figure 2. For better visualization, only a matrix of 29×29 pixels around the wire tip is depicted. Negative values indicate a decrease in intensity after using the TSE sequence due to an increase in temperature around the wire tip. Similar observations were noticeable for five adjacent slices in the images obtained using TrueFISP but not in the images obtained using the FLASH sequence.

Figure 3 shows a box plot of the pixel value distributions presented in (Figure 2) and normalized to the mean intensity of the

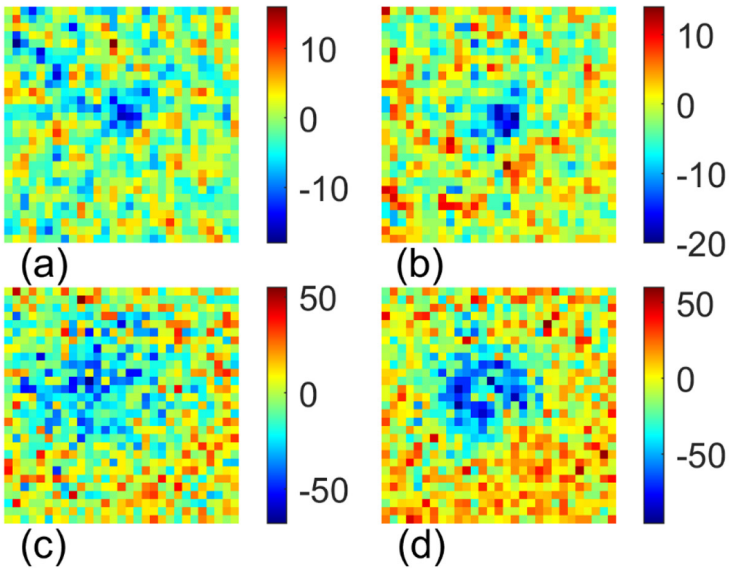

Figure 2: (**a**), (**b**) Difference images using Fast Low-Angle Shot sequence and (**c**), (**d**) True Fast Imaging with Steady Precession sequence. (**b**), (**d**) are related to the slice containing the wire tip, and (**a**), (**c**) represent the adjacent slice.

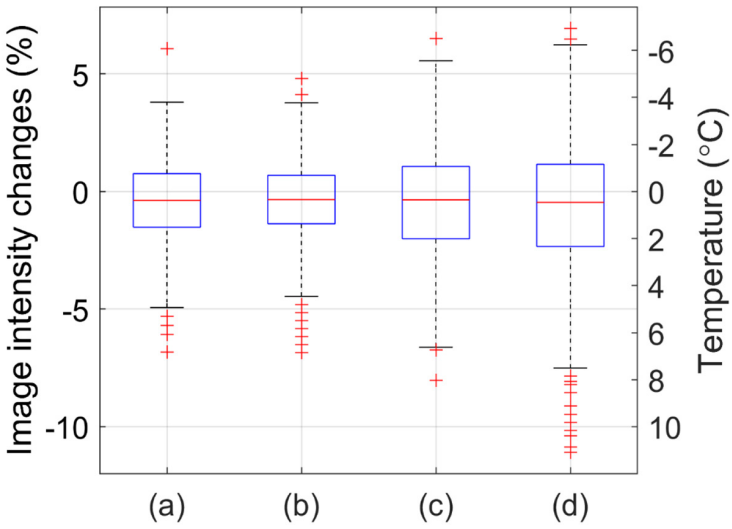

Figure 3: (**a**), (**b**) Box plots of the relative change in pixel value distributions for the different images obtained from Fast Low-Angle Shot and (**c**), (**d**) True Fast Imaging with Steady Precession. (**b**), (**d**) represent the data from the slice containing the wire tip, and (**a**), (**c**) represent the data from the adjacent slice.

corresponding reference images. The median and the first and third quartiles are displayed with horizontal lines of the boxes. The length of the vertical lines (whisker) is 1.5 times the interquartile values. The outliers (values outside the whisker length) are mostly placed on the negative side, showing a decrease in intensity for pixels around the wire. If we consider T_1 to change with temperature with a factor of 1.3% / °C for the proposed phantom [13], the estimation of the temperature based on the changes in signal intensity is possibly presented on the right-hand side of Figure 3.

Second approach

Images acquired at different TI values exhibited changes in quality. The FLASH showed noisy images at some TI values, and a visually detectable pattern of T_1 change near the wire was not observed. TrueFISP images were affected by the banding artifact. A T_1 map of the phantom obtained using TrueFISP is depicted in Figure 4. Several pixel values were adjusted for a better contrast at the bottom. The wire tip is placed at the center of the image. For a temperature estimation, the T_1 relative change in each pixel was calculated as the difference between the T_1 value of that pixel and a mean value divided by the mean value ($\Delta T_1/T_1$). The mean value of T_1 calculated from a rectangular area of 144 pixels outside the wire region was 1123±12 ms. Temperature dependence of the order of 1.3% / °C for the proposed phantom [13] was considered for temperature estimation.

Discussion

A phantom with a metal wire inside was built to resemble a brain tissue with a DBS electrode inside. MRI-induced heating near the wire tip was estimated using T_1 thermometry. Two approaches were considered as follows: 1) a high SAR sequence (TSE) was introduced to increase the generated heat; a temperature map was produced from a subtraction image, showing the difference in the signal intensity before and immediately after applying the TSE sequence and 2) a temperature map was

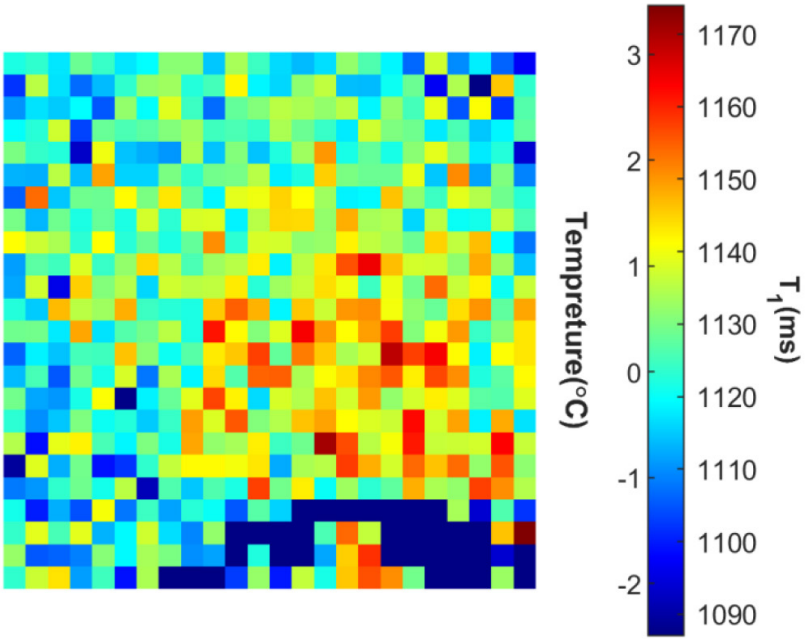

Figure 4: A T_1 map obtained from True Fast Imaging with Steady Precession (TrueFISP). Several pixel values at the bottom of the image were adjusted for better contrast. A temperature estimation is also provided based on the relative change in T_1.

obtained from a T_1 map near the wire. However, FLASH and TrueFISP were used for both approaches, the TrueFISP showed better performance for both approaches in terms of a clear pattern of intensity changes near the wire with superior spatial resolution and in a shorter acquisition time. The results show that the TrueFISP might be a good candidate for thermal field estimation near electrodes in phantoms for both approaches. The use of a T_1 map obtained from TrueFISP leads to determining induced heat from the imaging sequence. Such temperature maps help develop new protocols for the safe MRI of these patients.

For the subtraction method, the TrueFISP provided images with the best visual quality, acceptable spatial resolution ($1\times1\times1.5$ mm^3), and shorter acquisition times compared with that of FLASH ($1\times1\times3$ mm^3), probably due to the higher signal intensity of TrueFISP sequence in comparison to that of the FLASH [15]. For TrueFISP, the SNR is almost independent of *TR* for very short *TRs* [28], resulting in high-quality images in very short acquisition periods. The susceptibility artifact is always present, and from the artifact perspective, TrueFISP with a phase evolution similar to spin echoes [16] provides the best option for implant MRI. However, pixel values for TrueFISP were more scattered compared with those of FLASH (Figure 3), which could be due to reduced slice thickness for TrueFISP.

During the TSE sequence, the quick heating [18] resulted in considerable heat dissipation before the acquisition of the second image. Thermal models [18] are suggested for pixels near the wire for both the dynamic changes in temperature and the susceptibility artifact, which may conceal potentially harmful hot spots next to the electrodes.

Magnetic resonance thermometry using heating pulses [17, 32] or high SAR sequences [18] provides an extreme condition, in which an extra amount of heat is produced. Despite several advantages, such as controlled implant heating, this method is inappropriate for real situations in which implanted patients are exposed to an imaging sequence. On the other hand, T_1 mapping performed by a few repetitions of a low SAR sequence seems more suitable in this application because a T_1 map can be converted to a temperature map for a specific ROI. In this study, the temperature map obtained from the T_1 map showed a temperature increase of almost 1 °C, directly related to the imaging sequence without using a high SAR sequence (Figure 4). A high SAR sequence may elevate the temperature increase to several degrees Celsius as shown in Figure 3.

In the present study, the small size of the phantom could intensify the effect of the susceptibility artifact. Therefore, experiments using a head phantom or animals with implanted DBS electrodes are recommended. However, obtained results can be considered criteria to compare various situations and methods based on the temperature in DBS patients.

Conclusion

The TrueFISP shows superior potential for T_1 thermometry in implant MRI regarding the spatial resolution and acquisition time compared with that of FLASH. The TrueFISP is not usually recognized as a neuroimaging sequence. However it can provide a higher SNR, and reduced susceptibility artifact leading to a promising sequence in advanced applications, such as T_1 thermometry and mapping for patients with DBS electrodes.

Acknowledgment

The authors wish to thank Dr. K. Abdi from the instrumental analysis lab, school of pharmacy, Tehran University of Medical Sciences; Ms. M. Pakravan from the department of medical physics and biomedical engineering, Tehran University of Medical Sciences; Mr. M. Mollazadeh from MRI center, Shariati Hospital; and Antenna Laboratory, School of Electrical and Computer Engineering, the University of Tehran for their kind help in this

work. The authors would like to acknowledge National Brain Mapping Laboratory (NBML), Tehran, Iran, for providing data acquisition service for this research work.

Authors' Contribution

Z. Zarrini-Monfared was involved in material preparation, data collection and analysis, and writing the first draft of the manuscript. M. Parvaresh conceived the idea and read and approved the final manuscript. MM. Mirbagheri conceived the idea and was involved in material preparation, data collection and analysis, and reviewing the manuscript. All the authors read, modified, and approved the final version of the manuscript.

Ethical Approval

This study was approved by the ethics committee at Tehran University of Medical Sciences with the ethical code IR.TUMS.MEDICINE.REC.1398.916.

Funding

The author(s) disclosed receipt of the following financial support for the research of this article: This work was supported by the Tehran University of Medical Sciences, Tehran, Iran [grant number TUMS-40502].

Conflict of Interest

None

References

1. Middlebrooks EH, Domingo RA, Vivas-Buitrago T, Okromelidze L, Tsuboi T, Wong JK, et al. Neuroimaging Advances in Deep Brain Stimulation: Review of Indications, Anatomy, and Brain Connectomics. *AJNR Am J Neuroradiol.* 2020;**41**(9):1558-68. doi: 10.3174/ajnr.A6693. PubMed PMID: 32816768. PubMed PMCID: PMC7583111.
2. Xiao Y, Lau JC, Hemachandra D, Gilmore G, Khan AR, Peters TM. Image Guidance in Deep Brain Stimulation Surgery to Treat Parkinson's Disease: A Comprehensive Review. *IEEE Trans Biomed Eng.* 2021;**68**(3):1024-33. doi: 10.1109/TBME.2020.3006765. PubMed PMID: 32746050.
3. Rezai AR, Phillips M, Baker KB, Sharan AD, Nyenhuis J, Tkach J, et al. Neurostimulation system used for deep brain stimulation (DBS): MR safety issues and implications of failing to follow safety recommendations. *Invest Radiol.* 2004;**39**(5):300-3. doi: 10.1097/01.rli.0000124940.02340.ab. PubMed PMID: 15087724.
4. Medtronics I. MRI guidelines for medtronic deep brain stimulation systems. 2015. Available from: https://mriquestions.com/uploads/3/4/5/7/34572113/dbs_medtronics_contrib_228155.pdf.
5. Larson PS, Richardson RM, Starr PA, Martin AJ. Magnetic resonance imaging of implanted deep brain stimulators: experience in a large series. *Stereotact Funct Neurosurg.* 2008;**86**(2):92-100. doi: 10.1159/000112430. PubMed PMID: 18073522.
6. Zrinzo L, Yoshida F, Hariz MI, Thornton J, Foltynie T, Yousry TA, Limousin P. Clinical safety of brain magnetic resonance imaging with implanted deep brain stimulation hardware: large case series and review of the literature. *World Neurosurg.* 2011;**76**(1-2):164-72. doi: 10.1016/j.wneu.2011.02.029. PubMed PMID: 21839969.
7. Baker KB, Tkach JA, Nyenhuis JA, Phillips M, Shellock FG, Gonzalez-Martinez J, Rezai AR. Evaluation of specific absorption rate as a dosimeter of MRI-related implant heating. *J Magn Reson Imaging.* 2004;**20**(2):315-20. doi: 10.1002/jmri.20103. PubMed PMID: 15269959.
8. Nitz WR, Brinker G, Diehl D, Frese G. Specific absorption rate as a poor indicator of magnetic resonance-related implant heating. *Invest Radiol.* 2005;**40**(12):773-6. doi: 10.1097/01.rli.0000185898.59140.91. PubMed PMID: 16304480.
9. Mattei E, Triventi M, Calcagnini G, Censi F, Kainz W, Mendoza G, Bassen HI, Bartolini P. Complexity of MRI induced heating on metallic leads: experimental measurements of 374 configurations. *Biomed Eng Online.* 2008;**7**:11. doi: 10.1186/1475-925X-7-11. PubMed PMID: 18315869. PubMed PMCID: PMC2292730.
10. Rieke V, Butts Pauly K. MR thermometry. *J Magn Reson Imaging.* 2008;**27**(2):376-90. doi: 10.1002/jmri.21265. PubMed PMID: 18219673. PubMed PMCID: PMC2780364.

11. Winter L, Oberacker E, Paul K, Ji Y, Oezerdem C, Ghadjar P, et al. Magnetic resonance thermometry: Methodology, pitfalls and practical solutions. *Int J Hyperthermia.* 2016;**32**(1):63-75. doi: 10.3109/02656736.2015.1108462. PubMed PMID: 26708630.
12. Saleh C, Dooms G, Berthold C, Hertel F. Post-operative imaging in deep brain stimulation: A controversial issue. *Neuroradiol J.* 2016;**29**(4):244-9. doi: 10.1177/1971400916639960. PubMed PMID: 27029393. PubMed PMCID: PMC4978322.
13. Detti V, Grenier D, Perrin E, Beuf O. Assessment of radiofrequency self-heating around a metallic wire with MR T1-based thermometry. *Magn Reson Med.* 2011;**66**(2):448-55. doi: 10.1002/mrm.22834. PubMed PMID: 21360744.
14. Allison J, Yanasak N. What MRI Sequences Produce the Highest Specific Absorption Rate (SAR), and Is There Something We Should Be Doing to Reduce the SAR During Standard Examinations? *AJR Am J Roentgenol.* 2015;**205**(2):W140. doi: 10.2214/AJR.14.14173. PubMed PMID: 26204302.
15. Hargreaves BA. Rapid gradient-echo imaging. *J Magn Reson Imaging.* 2012;**36**(6):1300-13. doi: 10.1002/jmri.23742. PubMed PMID: 23097185. PubMed PMCID: PMC3502662.
16. Scheffler K, Hennig J. Is TrueFISP a gradient-echo or a spin-echo sequence? *Magn Reson Med.* 2003;**49**(2):395-7. doi: 10.1002/mrm.10351. PubMed PMID: 12541263.
17. Ehses P, Fidler F, Nordbeck P, Pracht ED, Warmuth M, Jakob PM, Bauer WR. MRI thermometry: Fast mapping of RF-induced heating along conductive wires. *Magn Reson Med.* 2008;**60**(2):457-61. doi: 10.1002/mrm.21417. PubMed PMID: 18570323.
18. Shrivastava D, Abosch A, Hughes J, Goerke U, DelaBarre L, Visaria R, et al. Heating induced near deep brain stimulation lead electrodes during magnetic resonance imaging with a 3 T transceive volume head coil. *Phys Med Biol.* 2012;**57**(17):5651-65. doi: 10.1088/0031-9155/57/17/5651. PubMed PMID: 22892760. PubMed PMCID: PMC3469254.
19. Wansapura JP, Holland SK, Dunn RS, Ball WS Jr. NMR relaxation times in the human brain at 3.0 tesla. *J Magn Reson Imaging.* 1999;**9**(4):531-8. doi: 10.1002/(sici)1522-2586(199904)9:4<531::aid-jmri4>3.0.co;2-l. PubMed PMID: 10232510.
20. Scheffler K, Hennig J. T(1) quantification with inversion recovery TrueFISP. *Magn Reson Med.* 2001;**45**(4):720-3. doi: 10.1002/mrm.1097. PubMed PMID: 11284003.
21. Shellock FG. Patient monitoring in the magnetic resonance environment. In: Magnetic resonance procedures: health effects and safety. Boca Raton: CRC Press, 2001. p. 217-40.
22. Kato H, Kuroda M, Yoshimura K, Yoshida A, Hanamoto K, Kawasaki S, et al. Composition of MRI phantom equivalent to human tissues. *Med Phys.* 2005;**32**(10):3199-208. doi: 10.1118/1.2047807. PubMed PMID: 16279073.
23. Armenean C, Perrin E, Armenean M, Beuf O, Pilleul F, Saint-Jalmes H. RF-induced temperature elevation along metallic wires in clinical magnetic resonance imaging: influence of diameter and length. *Magn Reson Med.* 2004;**52**(5):1200-6. doi: 10.1002/mrm.20246. PubMed PMID: 15508156.
24. Bhusal B, Nguyen BT, Vu J, Elahi B, Rosenow J, Nolt MJ, et al. Device Configuration and Patient's Body Composition Significantly Affect RF Heating of Deep Brain Stimulation Implants During MRI: An Experimental Study at 1.5T and 3T. *Annu Int Conf IEEE Eng Med Biol Soc.* 2020;**2020**:5192-7. doi: 10.1109/EMBC44109.2020.9175833. PubMed PMID: 33019155.
25. Golestanirad L, Angelone LM, Iacono MI, Katnani H, Wald LL, Bonmassar G. Local SAR near deep brain stimulation (DBS) electrodes at 64 and 127 MHz: A simulation study of the effect of extracranial loops. *Magn Reson Med.* 2017;**78**(4):1558-65. doi: 10.1002/mrm.26535. PubMed PMID: 27797157. PubMed PMCID: PMC5411348.
26. Cabot E, Lloyd T, Christ A, Kainz W, Douglas M, Stenzel G, et al. Evaluation of the RF heating of a generic deep brain stimulator exposed in 1.5 T magnetic resonance scanners. *Bioelectromagnetics.* 2013;**34**(2):104-13. doi: 10.1002/bem.21745. PubMed PMID: 23060256.
27. Deoni SC. High-resolution T1 mapping of the brain at 3T with driven equilibrium single pulse observation of T1 with high-speed incorporation of RF field inhomogeneities (DESPOT1-HIFI). *J Magn Reson Imaging.* 2007;**26**(4):1106-11. doi: 10.1002/jmri.21130. PubMed PMID: 17896356.
28. Liang Z-P, Lauterbur PC. Principles of magnetic resonance imaging: a signal processing per-

spective. New York, NY: IEEE Press; 2000.

29. Barral JK, Gudmundson E, Stikov N, Etezadi-Amoli M, Stoica P, Nishimura DG. A robust methodology for in vivo T1 mapping. *Magn Reson Med*. 2010;**64**(4):1057-67. doi: 10.1002/mrm.22497. PubMed PMID: 20564597. PubMed PMCID: PMC2962940.
30. Ogg RJ, Kingsley PB. Optimized precision of inversion-recovery T1 measurements for constrained scan time. *Magn Reson Med*. 2004;**51**(3):625-30. doi: 10.1002/mrm.10734. PubMed PMID: 15004808.
31. Deichmann R. Fast high-resolution T1 mapping of the human brain. *Magn Reson Med*. 2005;**54**(1):20-7. doi: 10.1002/mrm.20552. PubMed PMID: 15968665.
32. Gensler D, Fidler F, Ehses P, Warmuth M, Reiter T, Düring M, et al. MR safety: fast T1 thermometry of the RF-induced heating of medical devices. *Magn Reson Med.* 2012;**68**(5):1593-9. doi: 10.1002/mrm.24171. PubMed PMID: 22287286.